Lethaia
AN INTERNATIONAL JOURNAL OF PALAEONTOLOGY AND STRATIGRAPHY

The Sirius Passet Lagerstätte: silica death masking opens the window on the earliest matground community of the Cambrian explosion

KATIE M. STRANG, HOWARD A. ARMSTRONG, DAVID A. T. HARPER AND JOÃO P. TRABUCHO-ALEXANDRE

LETHAIA

Strang, K.M., Armstrong, H.A., Harper, D.A.T. & Trabucho-Alexandre, J.P. 2016: The Sirius Passet Lagerstätte: silica death masking opens the window on the earliest matground community of the Cambrian explosion. *Lethaia*, Vol. 49, pp. 631–643.

The Sirius Passet Lagerstätte (SP), Peary Land, North Greenland, occurs in black slates deposited at or just below storm wave base. It represents the earliest Cambrian microbial mat community with exceptional preservation, predating the Burgess Shale by 10 million years. Trilobites from the SP are preserved as complete, three-dimensional, concave hyporelief external moulds and convex epirelief casts. External moulds are shown to consist of a thin veneer of authigenic silica. The casts are formed from silicified cyanobacterial mat material. Silicification in both cases occurred shortly after death within benthic cyanobacterial mats. Pore waters were alkali, silica-saturated, high in ferric iron but low in oxygen and sulphate. Excess silica was likely derived from remobilized biogenic silica. The remarkable siliceous death mask preservation opens a new window on the environment and location of the Cambrian Explosion. This window closed with the appearance of abundant mat grazers later as the Cambrian Explosion intensified. ☐ *Cyanobacteria, depositional environment, silicification, Sirius Passet Lagerstätte, trilobite taphonomy.*

Katie M. Strang [k.m.strang@durham.ac.uk], Howard A. Armstrong [h.a.armstrong@durham.ac.uk], and David A. T. Harper [david.harper@durham.ac.uk], Department of Earth Sciences, Palaeoecosystems Group, Durham DH1 1LE, UK; João P. Trabucho-Alexandre [j.trabucho@uu.nl], Institute of Earth Sciences Utrecht, Utrecht University, Budapestlaan 4 3584 CD Utrecht, The Netherlands; *manuscript received on 20/04/2015; manuscript accepted on 11/12/2015.*

The Cambrian Explosion records the diversification of complex, mainly bilaterian, animal body plans and the expansion of animal-based marine ecosystems (Butterfield 2003). Much of what we know about this event is recorded in a succession of black shale conservation Lagerstätten. The Sirius Passet (SP) is the oldest of these and is located in J.P. Koch Fjord, N. Greenland, at 82°47.6′N, 42°13.7′W (Fig. 1A) and during the Cambrian lay at approximately 10°S (Fig. 1B; Peel & Ineson 2011). The black slates have been mapped as the 'Transitional' Buen, previously interpreted as fine-grained turbidites (Peel & Ineson 2011). *Buenellus higginsi* is the most common macrofossil, indicative of the *Nevadella* Biozone in Laurentia, equivalent to the middle part of Stage 3 (lowest stage of Series 2; 520–535 Ma; see Babcock 2005).

The SP fauna is similar to that of the Burgess Shale, comprising ca. 50 species including trilobites, sponges, worms, halkieriids, lobopods and non-trilobite bivalved arthropods. The SP Lagerstätte predates the Burgess Shale (510 Ma) and Chengjiang biotas (520 Ma) and is therefore possibly the earliest example of high-fidelity, soft-tissue preservation in the Cambrian. As recognized from studies of other Lagerstätten, an understanding of taphonomy is crucial in aiding anatomical interpretations of the SP fauna and provides for a better understanding of the palaeoenvironment, community reconstruction and early diagenesis (e.g. Gaines & Droser 2005; Zhu *et al.* 2006).

Similarities have been drawn between the depositional setting of the Burgess Shale and SP, for example proximity to a submarine cliff line and supposed basinal, turbiditic sedimentation (Peel & Ineson 2011). These similarities have led to the untested inference that SP fossils show Burgess Shale-type preservation (Gaines *et al.* 2008; Peel & Ineson 2011). Burgess Shale-type preservation is defined as 'exceptionally preserved fossils whose primary taphonomic mode is one of non-mineralizing organisms preserved as carbonaceous compressions in fully marine sediments' (Butterfield 1995). In the Burgess Shale, the soft-bodied fossils are preserved as thin, multi-layered silvery films (Whittington 1980). Significant discussion has focused on the composition of the films. Are they predomi-

[The copyright line for this article was changed on April 28 after original online publication]

DOI 10.1111/let.12174

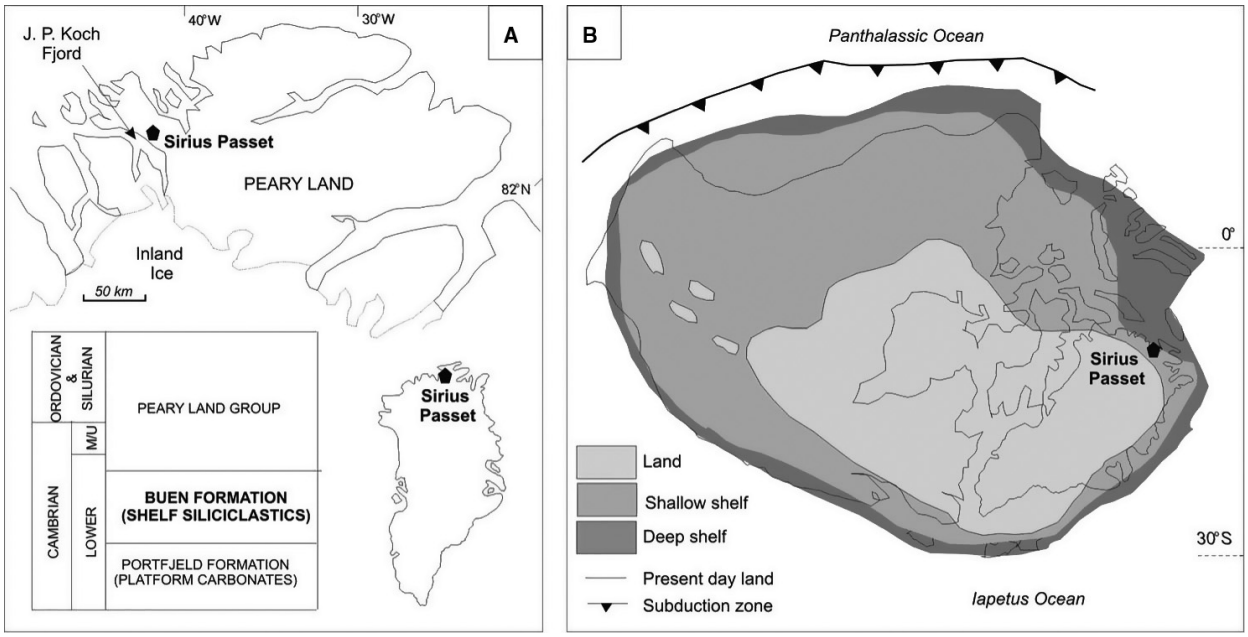

Fig. 1. A, Sirius Passet locality map, lithostratigraphy. B, Cambrian palaeogeography. Fig. 1B redrawn after Cocks and Torsvik (2011).

nantly organic and result from coalification during metamorphism (Butterfield 1990, 1995; Page *et al.* 2008) or predominantly composed of aligned clay minerals (Towe 1996; Orr *et al.* 1998)? Disagreement regarding the composition of the fossils has led to a lack of consensus regarding the mode of fossilization. Butterfield (1990, 1995) proposed that the clay which surrounded the fossils during burial acted as a catalyst that inhibited microbial decomposition of the labile tissues, leaving the organic material to be 'tanned' (Butterfield 1990) and producing a kerogen film during diagenesis. In comparison, Orr *et al.* (1998) concluded that fossilization occurred during decomposition as a consequence of chemical interactions between the tissues and the surrounding clays. In this model, variations in composition and reactivity of the different tissues during decomposition resulted in varying accumulations of clays on the carcass either by accumulation or direct precipitation from the pore water. The enhanced preservation of non-mineralized tissues may have also resulted from a combination of environmental factors. Near bottom anoxia would have prevented sediment irrigation by bioturbators. Reduced permeability of the seafloor and exclusion of oxygen may have also resulted from an absence of coarse grains such as silt, faecal pellets or bioclasts and the presence of reduced bottom waters that may have acted to deflocculate clay mineral aggregations and facilitated the precipitation of early diagenetic pore occluding carbonate cements (Gaines *et al.* 2005).

Some of the controversy surrounding the mechanisms of Burgess Shale-type preservation is in part due to the loss of primary features during post-depositional diagenesis and metamorphism. As a consequence of low greenschist facies metamorphism and cleavage formation, the phyllosilicates of the Burgess Shale currently associated with the fossils are not the same as the minerals that initially buried the fossils (Powell 2003). A detailed understanding of the metamorphic history and reconstruction of the primary bulk mineralogy of the Burgess Shale precludes the presence of highly reactive clay species necessary for the Butterfield model involving organic preservation due to clay-related suppression of decomposition-related reactions (Powell 2003). Instead, it indicates there was nothing unusual about the initial mud sediment and lends support to the Orr hypothesis of clay templating during decomposition (Powell 2003). This re-evaluation challenges the nature of Burgess Shale-type preservation and shows the importance of determining the mineralogical changes in Cambrian black shale Lagerstätten during metamorphism. This is critical for understanding the taphonomy, in which previous discussions of the SP, metamorphism has been largely ignored.

In this contribution, we use a combination of observations, petrography and SEM analyses to demonstrate the sequence of events leading to an early 'death mask' preservation of the trilobites within the SP and discount the influence of metamorphic processes. A key element of our proposed

trilobite taphonomy is the sealing of the specimens and early silicification, within the microbial mats on which they lived. This taphonomy though common in the Ediacaran is unique to the Cambrian and may only have existed for a short time due the absence of the mat grazing guild that appeared later in the Cambrian Explosion.

Methods

Samples were collected during expeditions to SP led by Harper in 2009 and 2011. Thin (25 μm) double-polished thin sections, cut perpendicular to bedding, provided petrographic and textural data. Samples were studied for texture and composition using optical microscopy and scanning electron microscopy. Prior to SEM imaging, all samples were coated with a ca. 20 nm layer of carbon.

SEM imaging and analysis were carried out using the Hitachi SU-70 FEG SEM in Durham University using secondary electron and backscattered electron detectors at 15 kV. Both primary and secondary backscatter techniques were used to produce general images prior to elemental mapping (SEM-EDAX) and SEM-CL analysis. EDAX was carried out using the backscatter detector and the same voltage settings used for imaging. For point analysis, a cobalt standard was run before analysis to confirm quantitative results, and Tables 1 and S2 (See supplementary information) provide detailed mineralogical data. This was performed using the QUANT software and running the standard several times to ensure maximum accuracy (100 $\pm$ 5%).

SEM-CL (cathodoluminescence) was carried out using a mirror-type detector (Gatan Mono-CL) based in Durham University (Department of Physics). The machine was set to low magnification with a 10 kV voltage to allow the site of interest to be determined. The working distance was set to 20 mm and then adjusted as necessary to allow focusing of the sample. Working distance is then set to 16.2–16.7 mm and CL luminosities collected. Results were obtained using both the panchromatic mode (mono-CL) with both mirrors adjusted to panchromatic settings and then each colour filter was inserted one by one (red >600 nm, green >480–580 nm, and blue <480 nm). For individual grain studies, mono-CL was used to produce grey-scale pictures rather than true colour RGB CL. The former is faster at producing images with textural details, especially at high magnification (Schieber *et al.* 2000). Various studies have been carried out which show that quartz grains display a variety of luminescence intensities dependent on their provenance. The standards used were adapted from Seyedolali *et al.* (1997) and Schieber *et al.* (2000). CL intensity is dependent on the density of intrinsic and extrinsic defects within the band gap of the mineral. These defects are usually structural imperfections in the quartz crystal due to vacancies within the crystal lattice. These include point defects, translations, radiation damage, shock damage, melt inclusions and fluid inclusions. These types of defects can provide information on the conditions during mineralization and subsequent post-mineralization events such as deformation and metamorphism (Frelinger *et al.* 2014). The results were compared to other quartz CL provenance data in the literature to identify the luminosities.

Bulk mineralogy was checked using XRD of the <2μ clay fraction following the standard procedures outlined by Moore & Reynolds (1997). Rock samples were gently disaggregated in an agate mortar and pestle to avoid shearing the clays. Organic matter was removed by leaving the sample in a solution of 5% hydrogen peroxide until reaction ceased. The sample was then centrifuged at 2000 rpm, before decanting the supernatant liquid. Distilled water was then added and the sample was stirred. This was repeated until the supernatant liquid was neutral and the clay no longer fluctuated. Separation of clay fraction and saturation for XRD analysis was carried out using the following procedure. About 5 ml of dispersion agent was added and the sample was stirred well before centrifuging for 84 seconds at 800 rpm. The supernatant liquid was decanted into another tube. These steps were repeated until the sample was clean. Separated clays were then air-dried and samples placed on coverslips. Samples were analysed in a Bruker D8 Advance Diffractometer. CuKα radiation counting ranged from 2 to 60°

Table 1. Bulk-rock chemistry (in wt. %) of the low-carbonate Burgess Shale metamudstones (Walcott Quarry, Raymond Quarry and Tuzoia Beds extracted from Powell 2003) compared with the bulk-rock chemistry of SP.

Wt. %	Walcott 1	Walcott 2	Raymond	Tuzoia	PAAS	Sirius Passet
SiO_2	53.71	50.34	50.10	50.63	62.8	63.46
Al_2O_3	24.11	23.32	21.25	24.54	18.90	26.61
K_2O	6.75	7.07	4.15	6.15	3.70	4.39
K/Al	0.280	0.303	0.195	0.250	0.196	0.165

2θ with a 0.02° 2θ steps at 0.85 seconds per step. Lower angles were run than in bulk analysis in order to see low-angle clay peaks. Standard d spacing was calculated following Moore & Reynolds (1997).

Results

Specimens

Buenellus specimens are preserved complete, in life position and in 3-D. Two types of preservation are shown: (1) concave external moulds comprise thin (<1 mm) veneers of silica (Fig. 2A); and (2) convex epirelief casts composed predominantly of silicified microbial mat material (Fig. 2B, C). The microbial mat occurs as aggregates of hollow, cell-like structures with only the cell wall mineralized. Two microbial textures are preserved: (1) the sheath, which consists of small (<5 μm) equidimensional cells and spherical vesicles up to 2 μm in diameter (Fig. 2D, E); and (2) tubular or dendritically branching microbial filaments (Fig. 2F), observed only on the surface of the fossils.

Sedimentary petrography

The cleavage parallels sedimentary bedding and primary sedimentary textures are preserved. Two end-member lithofacies are recognized, a 'spotted' and a silt-rich facies (Fig. 3). The 'spotted' facies consists of structureless to discontinuously laminated phyllosilicates containing Al-rich chlorite-mica aggregates that are 10–20 μm in diameter (Fig. 3A, B). Significantly, outsized clasts of silicified microbial mat occur infrequently in both the 'spotted' facies and the silt-rich facies (Fig. 3C). The silt-rich facies consists of clay to very fine silt particles composed predominantly of phyllosilicates with minor detrital quartz grains in the silt fraction (Fig. 3D, E). Outsized, lenticular mud clasts are present in a few beds (Fig. 3F). Bedsets are planar and cross-laminated

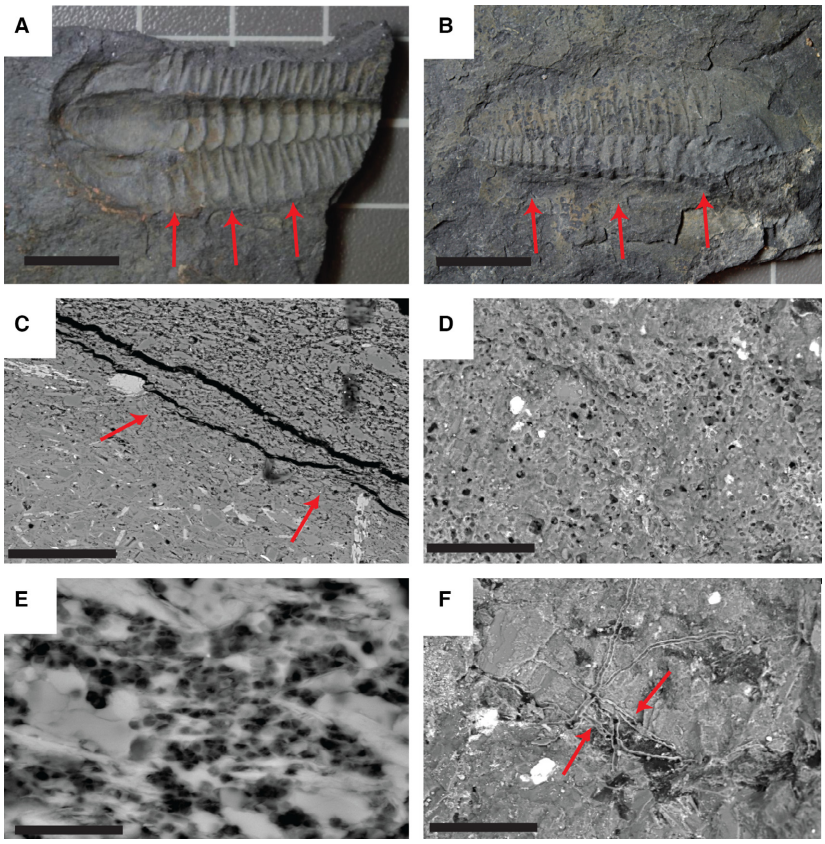

Fig. 2. High resolution photographs and SEM images. A, Image showing convex external mould of *Buenellus*; arrows indicate where thin sections were cut. Scale bar 1 cm. B, Convex epirelief cast of *Buenellus*; arrows indicate where thin sections were cut. Scale bar 1 cm. C, BSE SEM image showing matrix and microbial material; arrows indicate where mat material begins. Scale bar 1 cm. D, SE SEM image showing microbial mat material as aggregates of hollow, cell-like structures with only the cell wall mineralized, scale bar 1 cm. E, High magnification SEM BSE image showing 'webbed' silicified microbial mat structures. F, SEM SE image showing branching microbial filaments growing on the surface of the fossil. Scale bar 100 mm.

(Fig. 3G), with sharp to gradational boundaries between coarser and finer layers (Fig. 3H).

Bulk mineralogy

Bulk-rock composition is similar to that of average shale (Post-Archean Australian Shale (PAAS), but differs from the Burgess Shale or PAAS in higher detrital quartz, lower K/Al (0.165, see Supporting information) and an absence of calcite (Table 1). The mineral assemblage of chlorite–mica–quartz and minor/trace of carbon, albite and illite and the absence of sulphates is found to be stable from upper sub-greenschist to middle greenschist facies (Powell

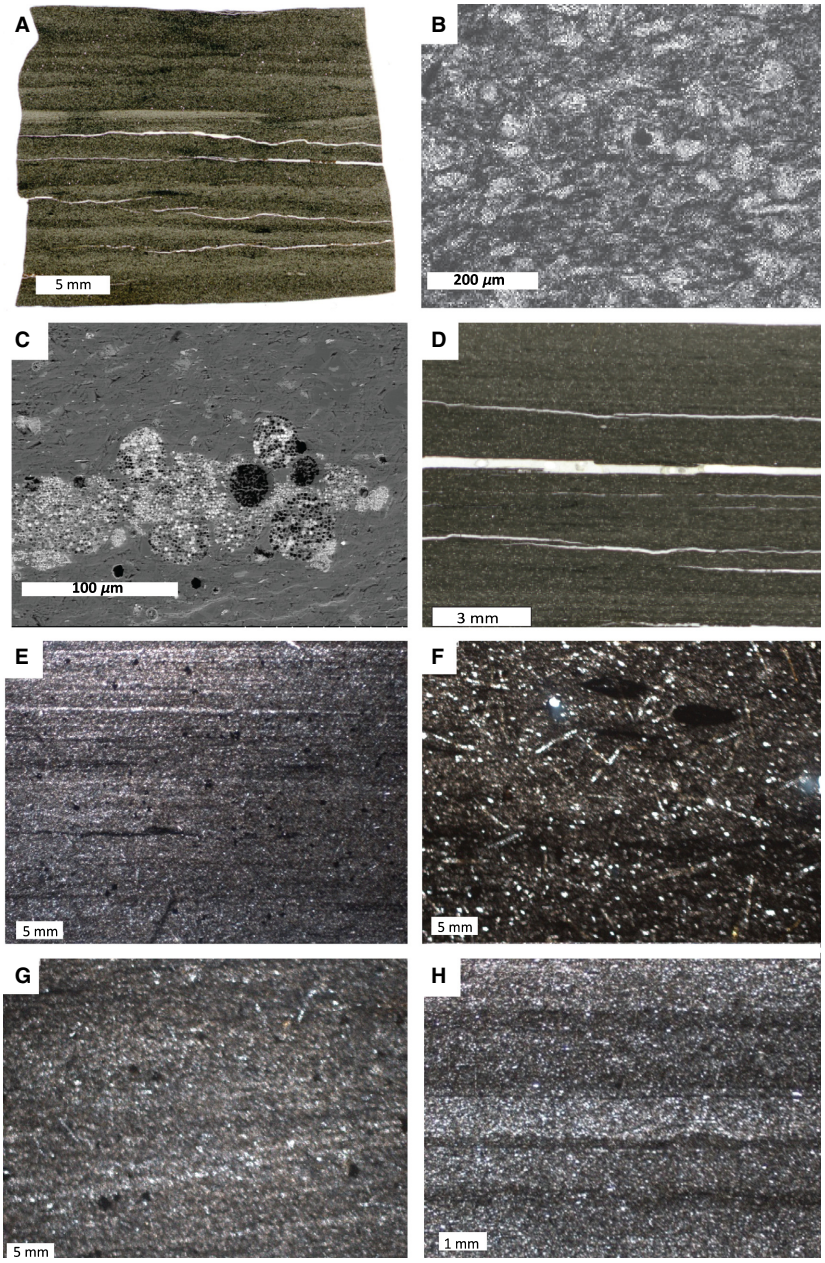

Fig. 3. Thin section photomicrographs; SEM and BSE images showing the different facies types. A, High resolution photomicrograph of a thin section showing the concentration of chlorite-mica aggregates into discontinuous wavy beds (3.4 m from base of log). B, Photomicrograph in plane polarized light showing chlorite-mica aggregates of varying sizes (1.12 m above base of log). C, BSE photomicrograph of silicified microbial mat fragment in the silt rich facies (5.5 m above base of log). D, Photomicrograph of a thin section showing laminated fabric and continuous and discontinuous silt layers (2.62 m from base of log). E, Photomicrograph in plane polarized light showing lamination picked out by single grain thickness layers of detrital quartz (4.56 m up from base of log). F, Photomicrograph in plane polarized light showing elliptical outsized floating grains of dark mudstone within a matrix of phyllosilicates, quartz, and chloritoid porphyroblasts (3.31 m above the base of log). G, Photomicrograph showing planar cross laminated bedsets. H, Photomicrograph of the silt rich facies showing sharp to gradational boundaries between course and fine layers.

2003). The absence of carbonate is a consequence of the sediment having passed through the smectite–illite transition (S-I; below). Abundant chloritoid porphyroblasts are indicative of low greenschist facies metamorphism (Higgins *et al.* 2001; equivalent to ~10 km burial) and their random orientation relative to bedding indicates relatively low-pressure conditions or possible formation during retrogressive regional metamorphism. Chloritoid is represented by the general formula $(Fe,Mg,Mn)Al_2SiO_5(OH)_2$ and occurs in high-Al, low-temperature metapelites (Halferdahl 1961). It is normally formed through the reaction of pyrophyllite, a phyllosilicate clay and chlorite-forming chloritoid, quartz and water. During this reaction, any excess silica can be precipitated as inclusions within the chloritoid. Quartz inclusions are common in the chloritoid needles and appear as irregular shaped grains within the needle.

Total organic carbon ranges from 0.5 to 1%. However, Raiswell & Berner (1986) documented an exponential loss of organic carbon relative to vitrinite reflectance in shales. Lower greenschist facies metamorphism would correspond to a minimum vitrinite reflectance of 5% (Kisch 1987). Projecting the Raiswell & Berner curve to a greenschist facies equivalent yields an estimated organic carbon preservation of 15%. The initial organic carbon content of the SP would therefore have been >3%, a value typical for many oil source rocks.

SEM-EDAX

Quantitative elemental mapping across a convex epirelief cast of *Buenellus* (Fig. 4A) shows typical values for Si (84%), Al (11%) and Fe (5%) compared with the matrix (Supporting Information Tables S1–S3). There is evidence of small framboidal pyrite associated with the mat material, which is absent from the matrix (Fig. 4B).

SEM-CL

Panchromatic cathodoluminescence analysis shows the presence of two quartz phases. Detrital quartz grains in the matrix exhibit true colour RGB-CL brown shade of luminescence at around 540–550 nm (Fig. 4C). Silica in the mineralized mat and concave external moulds exhibits almost no luminescence (Fig. 4D). Mono-CL of metamorphic quartz grains found as inclusions within the chloritoid needle shows medium grey luminosity and a mottled texture (Fig. 4E). These were compared with individual grains of silica associated with the fossils, which exhibit no luminosity under mono-CL and appear black and textureless (Fig. 4D).

Discussion

Marine carbonaceous shales in the Cambrian were limited to shallow-water regions with turbulent circulation (Raiswell & Berner 1986). The presence in the SP of normal and reverse grading, scouring and cross-lamination indicates deposition from low-density sediment gravity flows at or just below storm wave base. Cross-lamination suggests sediment transport by ripple migration. Compacted mud ripples have been observed as extremely low-angle cross-lamination in ancient mudstones (Komárek & Anagnostidis 1986) and are consistent with sediment transport by mud-laden sediment gravity flows (Kremer & Kazmierczak 2005). The presence of oversized clasts in the normally graded sediment suggests flows had sufficient competence to transport larger clasts, such as a denser, mud-rich 'slurry-flow', transitional between a turbidity current and a debris flow (Komárek & Anagnostidis 1986).

The chlorite–mica aggregates in the spotted facies could have originated as primary detrital grains modified during weathering and transport or, formed as the result of diagenetic or metamorphic minerals mimicking existing sedimentary textures (see Craig *et al.* 2009). Aggregates are concentrated into discontinuous beds. These beds are sharp-based, normally graded with scour fills and faint cross-lamination. The aggregates were probably transported and size-sorted at the seafloor. Normal grading suggests deposition was from sediment gravity flows producing successive beds of rapidly accumulated sediment (Best 2005). The fabric is primary and the texture produced by metamorphism is inherited from a pre-existing sedimentary texture. Today, aggregates are produced largely by the activities of organisms living in the water column (e.g. through filter feeding, faecal pellet production, test building) or random collisions between grains in the water column (McCave 1985). The dense accumulations of pellets suggest these were originally hemipelagites deposited during quiescent periods.

If an average uncompacted thickness of 50 m (10 m compacted) for the SP and an age span of ca. 3 myr for the interval are taken, then a minimum average, long-term sedimentation rate of about 15 mm/kyr is realistic. We infer that this high sedimentation rate improved the chance of the fossils being buried, isolating them from the oxidizing environment at the seafloor. Given the lack of penetrative burrowing, it is likely that pore waters were already anoxic a few millimetres below the seafloor.

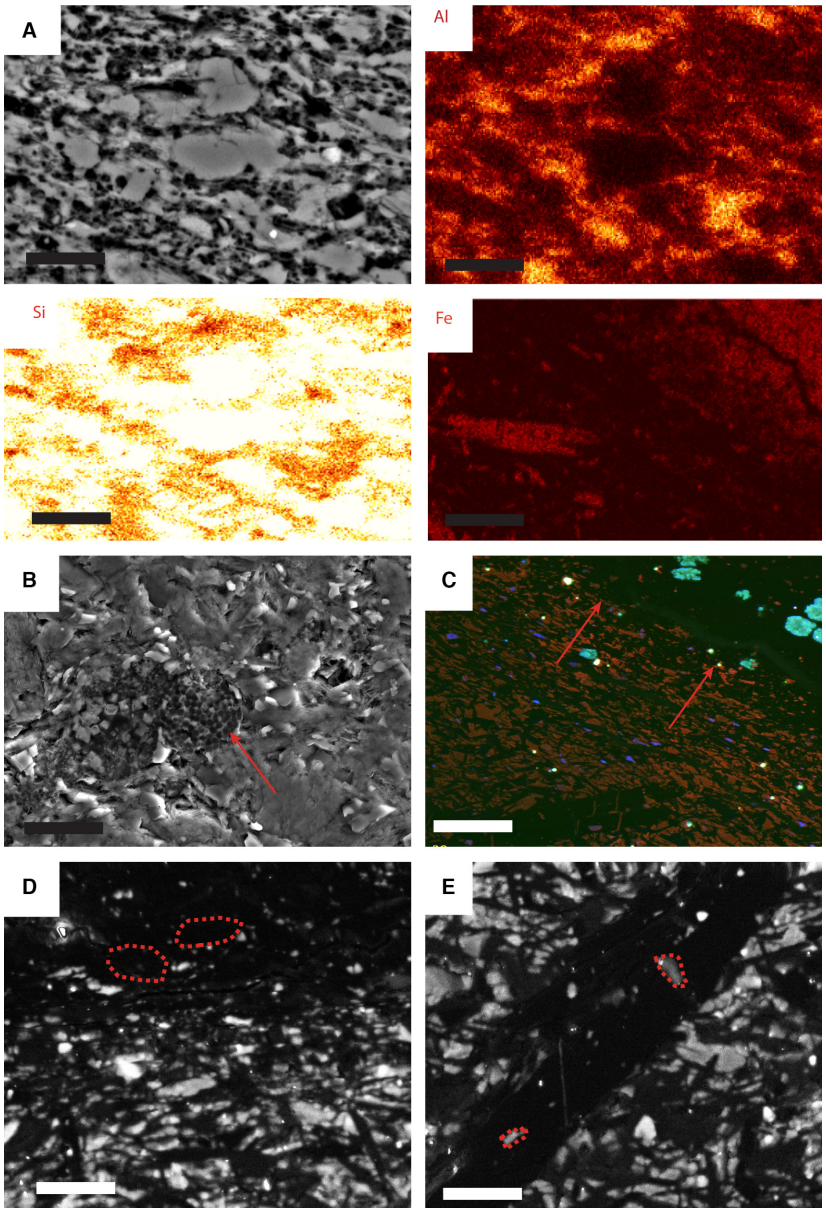

Fig. 4. A, elemental maps (top left SEM image to show locality of maps) taken across the mat material. Al, Si and Fe maps shown, notice the abundance of silica. Scale bar – 20 μm. B, BSE SEM image showing framboidal pyrite associated with the mat material. Scale bar 30 μm. C, RGB true colour CL showing brown shades of luminescence in the matrix, above arrows indicate area of mat material which has a distinctly different luminosity. D, mono-CL image, bottom half of image is matrix, whereas the top shows microbial material. Grains of non-luminescing silica associated with the fossils have been outlined (dashed line). Scale bar 20 μm. E, mono-CL image of chloritoid needle. Inclusions of metamorphic silica showing medium grey luminosity are outlined (dashed line). Scale bar 10 μm.

In modern pericontinental shelves, distance from shore is a good proxy for water depth. The SP pericontinental shelf was much wider than modern analogues (Fig. 5). Due to their distance from shore, distal, yet shallow-water deposits on wide shelves may have biological and geochemical characteristics indicative of deeper-water facies. On very wide shelves, with sufficiently low seafloor gradients, incoming waves dissipate their energy well before reaching the shore (Keulegan & Krumbein 1949). This may explain why, despite the large fetch expected from the palaeogeographical setting of SP, the shallow seafloor would be little subjected to swell, thereby allowing mud deposition. The seafloor was also consolidated by mat-forming cyanobacteria shortly after deposition.

Similar storm-influenced environments are proposed for the dark grey to black laminated mudstones of the Emu Bay Shale (Jago *et al.* 2012), the Alum (Thickpenny & Leggett 1987) and Burgess

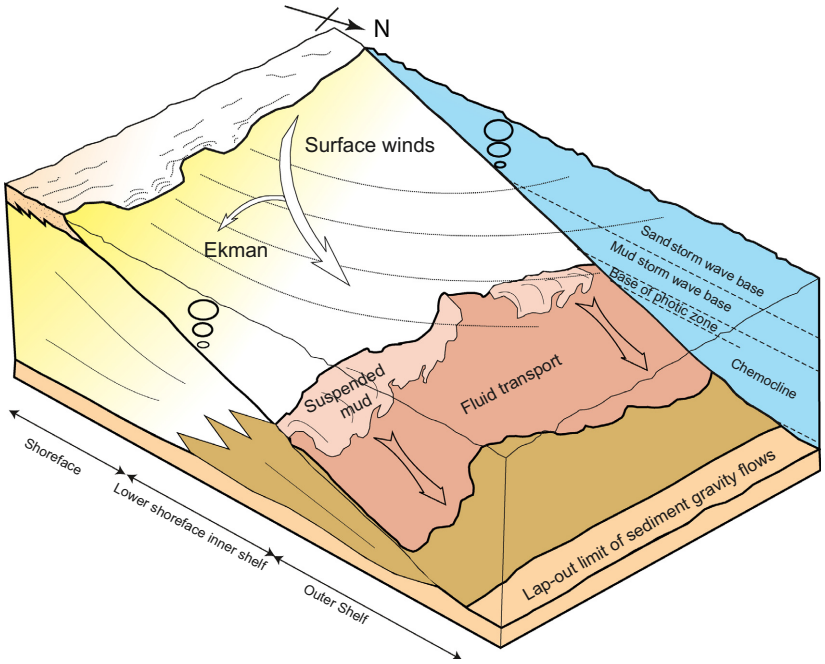

Fig. 5. Block diagram illustrating the depositional environment at Sirius Passet during the Early Cambrian (modified after Plint 2014).

Shales (Gabbott *et al.* 2008). In common with the SP, these deposits also lack penetrative bioturbation, suggesting anoxic conditions immediately below the seafloor. The presence of a diverse invertebrate benthos in the SP and an absence of pyrite framboids in the matrix indicate the lower water column was oxic with a sharp redox boundary at the sediment–water interface. Bioturbation is surficial and typically only occurs in association with generally large arthropod carcasses (Mangano *et al.* 2012). Benthic cyanobacteria were the dominant photoautotrophic and oxygenic microorganisms in the SP and could have produced or enhanced the oxygenated conditions at the seafloor. However, in extant cyanobacterial mats, sulphate reduction in the biomass can produce periodic hydrogen sulphide (H_2S) emissions above the mat surface, particularly at night (Jørgensen 1979). This could have been a major factor impeding the settlement of benthic organisms on the seafloor. The mat-dwelling fauna was ephemeral and either able to escape H_2S emissions or had adapted a resistance to short-lived H_2S toxicity. Occasional massive H_2S expulsion from the decaying mats might have led to mass mortalities of the mat-dwelling community (see also Weeks *et al.* 2002).

Microbial mat textures observed on the concave external moulds, epirelief convex casts and evidence of microbial mat growing over trilobites (see Mangano *et al.* 2012; fig. 1) indicate that the fauna was an autochthonous matground community previously only known from trace fossil evidence (Buatois *et al.* 2014).

The dense cellular aggregates comprising the microbial textures are compared with colonies of modern coccoid cyanobacteria, particularly with the exclusively benthic *Entophysalis* or *Chlorogloea* (e.g. Kremer & Kazmierczak 2005). The globular structures (Figs 2E, 3C) resemble the encapsulated aggregates of extant benthic coccoid cyanobacteria Pleurocapsales, particularly *Chroococcidiopsis* and *Stanieria* (Komárek & Anagnostidis 1986; Silva & Pienaar 2000; Kremer & Kazmierczak 2005). Similar structures have been documented from the Athel Silicyte in the South Oman Salt Basin, Sultanate of Oman by Rajaibi *et al.* (2015), and provide evidence of microbially mediated syndepositional precipitation of silica. These genera are known from freshwater and marine environments, and some pleurocapsaleans are adapted to low light levels within the photic zone (Stal & Walsby 2000). Similar material has been described from the Proterozoic (Gehling 1999) and Silurian (Kremer & Kazmierczak 2005). As cyanobacteria are a morphologically conservative group, SP specimens are probably part of the same groups.

We propose the arthropod-lobopodian fauna that characterizes the Sirius Passet inhabited a warm, muddy, matground habitat close to or just below storm wave base, but within the photic zone. We have found no evidence for aeolian deposition of clay or silt in the field or in our thin sections, in contrast to the study by Boudec *et al.* (2014). Primary productivity was principally by benthic cyanobacteria. Contemporary shallow subtidal to intertidal car-

bonate environments had a distinct shelly fauna including archaeocyathans, halkieriids, tommotiids, hyoliths, molluscs, rare trilobites, and a variety of other small shelly fossils of unknown affinity (examples cited in Mount & Signer 1985). The rapid appearance in the geological record and ecological stability of the 'Burgess Shale-type assemblages,' over some 10 million years, suggests that rather than being long-lived holdovers, successively displaced from the shallow water (Mount & Signer 1985; Morris 2009), these animals were members of new Bambachian megaguilds (groups of organisms with mutually similar adaptive strategies), highly specialized and adapted to the dynamic and unstable nature of the tropical, muddy lower shoreface and shelf (Fig. 5).

The three-dimensional preservation of cyanobacterial structure, the hyporelief external moulds and particularly the epirelief casts indicate the trilobite carapace remained intact long enough for the internal labile tissues to decompose and the body cavity to be injected with mat material. Dewatering and compaction occurs during early burial. Experimental and core studies indicate porosity in muds is reduced to 33–36% by 175 m depth. Effective porosity (~70%) is lost by 1 km depth of burial (Hedberg 1936). At the inferred sedimentation rates, specimens that had not been permineralized would have been flattened to one-third the original volume after 100 kyr–1 myr, thus providing sufficient time for early silicification and critically before the S-I transition between 1.8 and 3.7 km depth of burial. Major mineralogical changes with depth take place over the S-I transition (Hower *et al.* 1976). The most abundant mineral, illite/smectite, undergoes a conversion from less than 20% to about 80% illite layers over this interval, after which the proportion of illite layers remains constant. As the transition proceeds, illite packets grow within a shrinking matrix of smectite, dislocations decrease and pathways for ion transport are restricted, this causes a loss of local permeability and a rise in the fluid pressure gradient. Consequent loss of hydraulic continuity with the surface and a more efficient geopressure seals the clay to fluid flow (Freed & Peacor 1989). In the S-I transition, calcite decreases from about 20 percent of the rock to almost zero, disappearing from progressively larger size fractions with increasing depth; potassium feldspar (but not albite) decreases to zero; and chlorite appears to increase in amount. At these depths, smectite reacts with Al^{3+} and K^{+} from the decomposition of potassium feldspar to form illite with the release of Si^{4+}. Magnesium and iron lost from the smectite form chlorite and ultimately chloritoid. The stable clay mineral assemblage following the S-I transition is thus illite, quartz and chlorite. All the major mineralogical and chemical changes, as the response to burial and metamorphism, occurred in a closed system for all components except H_2O, CaO, Na_2O and CO_2 (Hower *et al.* 1976). Reactions during the S-I transition therefore explain the absence of calcite in the SP. The remaining reactions into lower greenschist facies metamorphism include conversion of remaining smectite to illite (up to ~175 °C) and the recrystallization of illite to micas (200–300 °C: Totten & Blatt 1993).

The timing of silicification is critical to understanding the taphonomic pathway. Silica supersaturation of pore fluids occurred due to the synsedimentary remobilization of biogenic silica; from silica released during the S-I transition or during greenschist facies metamorphism. Our key evidence for silicification being early, shortly after death includes the following:

1 The 3-D preservation of moulds and casts and cellular textures in the microbial mat material indicate silicification occurred before compaction and dewatering of the muds. The observation that 3-D cells are filled with monocrystalline quartz preserved within the cyanobacterial mat material indicates silica deposition prior to dewatering and compaction. Because the mat material is porous and the decay of labile cell contents occurred soon after death, it is unlikely that internal cell fluid pressure would have supported the primary structures on burial. Alternately, decay gasses from decomposition may have formed cavities (Reineck & Singh 1980) that prevented the collapse of the cells prior to silicification. A similar mechanism of mineral deposition in gas has been proposed for the formation of pyrite framboids in muds (e.g. Rickard 1970) and silica infilling of *Tasmanite* cysts (Schieber 1996). And the fact that spherical gas bubbles are found close to the sediment surface has been documented by Forstner *et al.* (1968). Silica deposition is therefore most likely to have occurred very early in diagenesis and within centimetres to decimetres of the sediment–water interface. At the proposed sedimentation rates for the SP, this would have been equivalent to a few thousand years of deposition;
2 The presence of synsedimentary rip-up clasts;
3 Microbial mat and convex external moulds are formed of non-luminescent, textureless silica.

Non-luminescing authigenic quartz lacks crystal lattice defects generated during metamorphism or volcanism (Seyedolali *et al.* 1997; Augustsson & Bahlburg 2003; Frelinger *et al.* 2014);

4 Metamorphic quartz inclusions in the chloritoid needles exhibit strong luminosity with a smooth to mottled texture. This is distinctly different from the silica associated with the fossils; and

5 The fact that chloritoid needles cross-cut all other textures indicates metamorphism occurred after silicification.

The presence of very early diagenetic silica deposition excludes a silica source during the S-I transition and during diagenetic to low-grade metamorphic recrystallization of illite to muscovite mica. Further, the early and largely biogenic porosity within the SP muds was filled by silica and not calcium carbonate (compare data from the Wheeler Formation: Gaines *et al.* 2005). That chalcedony appears to have been the initial silica phase deposited in the voids is not unusual, first documented by Folk & Weaver (1952) and subsequently in numerous other studies (e.g. Heath & Moberly 1971; Meyers 1977; Frondel 1978; Milliken 1979; Noble & Van Stempvoort 1989). The presence of pyrite framboids in the mat material indicates sulphate reduction and that pyrite remained a stable phase through to greenschist facies metamorphism.

Decay experiments show that silica precipitates from low-pH pore waters in extracellular and intracellular environments within a mat (Krauskopf 1959), particularly when the pore fluids have reduced dissolved sulphate (Birnbaum & Wireman 1985; Schultze-Lam *et al.* 1995). Soluble silica, in the form of monosilicic acid, H_4SiO_4, dissociates to $H_3SiO_4^-$ at pH values above ca. 9.7 (Birnbaum & Wireman 1985; Arp *et al.* 2003). $H_3SiO_4^-$ is a highly soluble form of silicic acid, and it reacts with hydrogen ions to form SiO_2 (Rickert *et al.* 2002; fig. 3). Silica nucleation and precipitation is sensitive to iron content of bottom/pore water and, in early Cambrian seawater, Fe^{2+} appears to have been high relative to FeOOH (Muscente *et al.* 2014). We hypothesize that sediment–water was saturated in silica, high in Fe^{2+} and low in oxygen and sulphate. Localized pH reduction was associated with the decay-initiated silica nucleation and precipitation within the mat. Silica-saturated pore waters could have been derived from the siliciclastic mud, by remobilization of biogenic silica (e.g. sponge spicules), or from the overlying seawater.

Early silicification as a mechanism of exceptional preservation is rare outside volcanic hot springs and a number of hypotheses for silicification have been proposed: (1) direct precipitation into void spaces; (2) microbial mediated silica precipitation (Schultze-Lam *et al.* 1995; Yee *et al.* 2003); and (3) chemically mediated silica precipitation (Patwardhan *et al.* 2011). It has been shown that microbial surfaces do not directly nucleate silica mineral formation; however, they play an important role in the aggregation of polymeric silica and the deposition of silica colloids on microbial surfaces (Patwardhan *et al.* 2011). For example, in modern hot spring environments, silica sinters actively form in close spatial relation to microorganisms (Yee *et al.* 2003 and references therein). Decay compounds, proteins and amino acids are all known to affect the kinetics, surface area of material, pore structure and particle size and are therefore implicated in silicification (Perry & Keeling-Tucker 2003). At present, we cannot distinguish between the different mechanisms proposed for silicification and all may have been important.

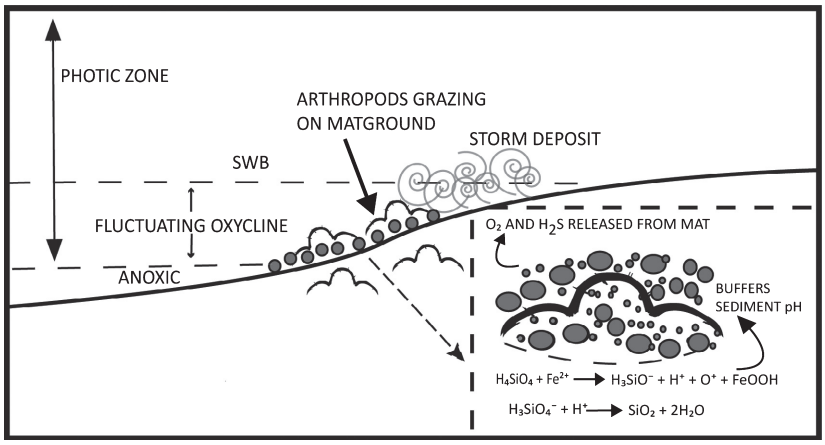

Fig. 6. Chemical pathways leading to the precipitation of silica and the reconstructed taphonomy of *Buenellus*.

Figure 6 shows our preferred taphonomic pathway. We propose that *Buenellus* was the dominant member of the matground community preserved in the SP. After death, the carapace was sealed by the growth of the microbial mat. During early burial, internal labile tissues decayed, and mat material was injected into the carcass to produce epirelief casts. The subsequent decay of the trilobite cuticle produced external moulds. All voids spaces were progressively infilled by silica as a consequence of localized pH reduction, associated with decay, occurring in the pore waters. Specimens were clearly permineralized, preserved in 3-D, before significant dewatering of the muds had taken place. Subsequent chemical reactions associated with the S-I transition and low greenschist facies metamorphism did not materially affect the preservation of the specimens.

Similar 'death mask' preservation has been described for the external moulds of soft-bodied Ediacaran biotas from the uppermost Proterozoic Rawnsley Quartzite, South Australia. However, in this example the sole veneer resulted from bacterial precipitation of iron minerals (Gehling 1999). A number of Cambrian Lagerstätten are characterized by pyritization of soft-bodied fossils, for example Chengjiang and Guanshan (Gabbott *et al.* 2004; Forchielli *et al.* 2014), secondary coating by iron (e.g. Emu Bay: Brett *et al.* 2009), or phosphatization (Zhu *et al.* 2014). Silica death mask preservation thus appears to be currently unique to the SP.

Conclusions

The arthropod-lobopodian fauna that characterizes the Sirius Passet inhabited a warm, muddy, matground habitat close to or just below storm wave base, but within the photic zone. Primary productivity was principally by benthic cyanobacteria. Trilobites from the SP are preserved as complete, concave hyporelief external moulds and convex epirelief casts. External moulds are shown to consist of a thin veneer of authigenic silica. The casts are silicified cyanobacterial mat material. Early silicification is supported by the presence of synsedimentary mat rip-up clasts, 3-D preservation, which indicates silicification prior to sediment compaction and textural and mono-CL evidence. The growth of metamorphic chloritoid needles, which cross-cut the silica in the matrix, indicates that metamorphism occurred much later. It is hypothesized that silicification was initiated by falling pH in the decaying mat. Pore waters are interpreted to have been initially alkali, silica-saturated, high in ferric iron but low in oxygen and sulphate. Excess silica was likely derived from remobilized biogenic silica, probably sponge spicules in the muddy sediment. Decay resulted in a lowering of pore water pH and the conditions necessary for silicification. It is not clear whether silicification was microbially or chemically mediated.

The remarkable preservation during very early silica mineralization provides a new window on the environment and location of the Cambrian Explosion. The iconic organisms of the Cambrian Explosion formed the first mat ground communities. At least in the case of the SP the presence of cyanobacterial mats, sealing both the sediments and fossils, was fundamental to the preservation of this community. With the rise of mat grazing organisms during the later Cambrian, this taphonomic window disappeared.

Acknowledgments. – Leon Bowen, Ian Chaplin, Chris Greenwell and Manohara Gv gave technical assistance. GEUS (Geological Survey of Denmark and Greenland), The Danish Council for Independent Research, Agouron Institute and the Carlsberg Foundation provided funding. Strang is in receipt of a NERC CASE Studentship (RF050232). The manuscript benefitted from the recommendations of two referees and careful editing by Dr A. W. Owen.

References

Arp, G., Reimer, A. & Reitner, J. 2003: Microbialite formation in seawater of increased alkalinity, Satonda Crater Lake, Indonesia. *Journal of Sedimentary Research 73*, 105–127.

Augustsson, C. & Bahlburg, H. 2003: Cathodoluminescence spectra of detrital quartz as provenance indicators for Paleozoic metasediments in southern Andean Patagonia. *Journal of South American Earth Sciences 16*, 15–26.

Babcock, L.E. 2005: Interpretation of biological and environmental changes across the Neoproterozoic-Cambrian boundary: developing a refined understanding of the radiation and preservational record of early multicellular organisms. *Palaeogeography, Palaeoclimatology, Palaeoecology 220*, 1–5.

Best, J. 2005: The fluid dynamics of river dunes: a review and some future research directions. *Journal of Geophysical Research 110*, F04S02.

Birnbaum, S.J. & Wireman, J.W. 1985: Sulfate-reducing bacteria and silica solubility: a possible mechanism for evaporite diagenesis and silica precipitation in banded iron formations. *Canadian Journal of Earth Sciences 22*, 1904–1909.

Boudec, A.L., Ineson, J., Rosing, M., Døssing, L., Martineau, F., Lécuyer, C. & Albarède, F. 2014: Geochemistry of the Cambrian Sirius Passet Lagerstätte, Northern Greenland. *Geochemistry, Geophysics, Geosystems 15*, 886–904.

Brett, C.E., Allison, P.A., DeSantis, M.K., Liddell, W.D. & Kramer, A. 2009: Sequence stratigraphy, cyclic facies, and Lagerstätten in the Middle Cambrian wheeler and Marjum formations, Great Basin, Utah. *Palaeogeography, Palaeoclimatology, Palaeoecology 277*, 9–33.

Buatois, L.A., Narbonne, G.M., Mángano, M.G., Carmona, N.B. & Myrow, P. 2014: Ediacaran matground ecology persisted into the earliest Cambrian. *Nature Communications 5*, 3544–3549.

Butterfield, N.J. 1990: Organic preservation of non-mineralizing organisms and the taphonomy of the burgess Shale. *Paleobiology 16*, 272–286.

Butterfield, N.J. 1995: Secular distribution of Burgess-Shale-type preservation. *Lethaia 28*, 1–13.
Butterfield, N.J. 2003: Exceptional fossil preservation and the Cambrian explosion. *Integrative and Comparative Biology 43*, 166–177.
Cocks, L.R.M. & Torsvik, T.H. 2011: The Palaeozoic geography of Laurentia and western Laurussia: a stable craton with mobile margins. *Earth-Science Reviews 106*, 1–51.
Craig, J., Fitches, W.R. & Maltman, A.J. 2009: Chlorite-mica stacks in low-strain rocks from central Wales. *Geological Magazine 119*, 243–256.
Folk, R.L. & Weaver, C.E. 1952: A study of the texture and composition of chert. *American Journal of Science 250*, 498–510.
Förstner, U., Müller, G. & Reineck, H. 1968: Sedimente und Sedimentgefüge des Rheindeltas im Bodensee. *Neues Jahrbuch für Mineraralogie Abh. 109*, 33–62.
Forchielli, A., Steiner, M., Kasbohm, J., Hu, S. & Keupp, H. 2014: Taphonomic traits of clay-hosted early Cambrian Burgess Shale-type fossil Lagerstätten in South China. *Palaeogeography, Palaeoclimatology, Palaeoecology 398*, 59–85.
Freed, R.L. & Peacor, D.R. 1989: Geopressured shale and sealing effect of smectite to illite transition. *AAPG Bulletin 73*, 1223–1232.
Frelinger, S.N., Ledvina, M.D., Kyle, J.R. & Zhao, D. 2014: Scanning electron microscopy cathodoluminescence of quartz: principles, techniques and applications in ore geology. *Ore Geology Reviews 65*, 840–852.
Frondel, C. 1978: Characters of quartz fibers. *American Mineralogist 63*, 17–27.
Gabbott, S.E., Xian-Guang, H., Norry, M.J. & Siveter, D.J. 2004: Preservation of Early Cambrian animals of the Chengjiang biota. *Geology 32*, 901–904.
Gabbott, S.E., Zalasiewicz, J. & Collins, D. 2008: Sedimentation of the phyllopod bed within the Cambrian Burgess Shale Formation of British Columbia. *Journal of the Geological Society 165*, 307–318.
Gaines, R.R. & Droser, M.L. 2005: New approaches to understanding the mechanics of Burgess Shale-type deposits: from the micron scale to the global picture. *The Sedimentary Record 3*, 4–8.
Gaines, R.R., Kennedy, M.J. & Droser, M.L. 2005: A new hypothesis for organic preservation of Burgess Shale taxa in the middle Cambrian Wheeler formation, House Range, Utah. *Palaeogeography, Palaeoclimatology, Palaeoecology 220*, 193–205.
Gaines, R.R., Briggs, D.E.G. & Yuanlong, Z. 2008: Cambrian Burgess Shale–type deposits share a common mode of fossilization. *Geology 36*, 755–758.
Gehling, J.G. 1999: Microbial mats in terminal Proterozoic siliciclastics: ediacaran death masks. *Palaios 14*, 40–57.
Halferdahl, L.B. 1961: Chloritoid: its composition, X-ray and optical properties, stability, and occurence. *Journal of Petrology 2*, 49–135.
Heath, G.R. & Moberly, R. Jr., 1971: Cherts from the western Pacific, Leg 7, Deep Sea Drilling Project. *In* Winterer E.L. & Riedel W.R., et al. (eds): *Initial Reports of the Deep Sea Drilling project*, *Volume 7*, U.S. Government Printing Office, Washington.
Hedberg, H.D. 1936: Gravitational compaction of clays and shales. *American Journal of Science 31*, 241–287.
Higgins, A.K., Leslie, A.G. & Smith, M.P. 2001: Neoproterozoic-Lower Palaeozoic stratigraphical relationships in the marginal thin-skinned thrust belt of the East Greenland Caledonides: comparisons with the foreland in Scotland. *Geological Magazine 138*, 143–160.
Hower, J., Eslinger, E.V., Hower, M.E. & Perry, E.A. 1976: Mechanism of burial metamorphism of argillaceous sediment: 1. Mineralogical and chemical evidence. *Geological Society of America Bulletin 87*, 725–737.
Jago, J.B., Gehling, J.G., Paterson, J.R. & Brock, G.A. 2012: Cambrian stratigraphy and biostratigraphy of the flinders ranges and the north coast of Kangaroo Island, South Australia. *Episodes 35*, 247–255.
Jørgensen, B. 1979: Diurnal cycle of oxygen and sulfide microgradients and microbial photosynthesis in a cyanobacterial mat sediment. *Applied and Environmental Microbiology 38*, 46–58.
Keulegan, G.H. & Krumbein, W.C. 1949: Stable configuration of bottom slope in a shallow sea and its bearing on geological processes. *Transactions, American Geophysical Union 30*, 855–861.
Kisch, H.J. 1987: Correlation between indicators of very low-grade metamorphism. *In* Frey M. (ed.): *Low Temperature Metamorphism*, 227–300. Blackie, Edinburgh.
Komárek, J. & Anagnostidis, K. 1986: Modern approach to the classification system of cyanophytes. 2-Chroococcales. *Archiv für Hydrobiologie Supplement 73*, 157–226.
Krauskopf, K.B. 1959: The geochemistry of silica in sedimentary environments. *Special Publications of SEPM 7*, 4–12.
Kremer, B. & Kazmierczak, J. 2005: Cyanobacterial mats from Silurian black radiolarian cherts: phototrophic life at the edge of darkness? *Journal of Sedimentary Research 75*, 897–906.
Mangano, M.G., Bromley, R.G., Harper, D.A.T., Nielsen, A.T., Smith, M.P. & Vinther, J. 2012: Nonbiomineralized carapaces in Cambrian seafloor landscapes (Sirius Passet, Greenland): opening a new window into early Phanerozoic benthic ecology. *Geology 40*, 519–522.
McCave, I.N. 1985: Recent shelf clastic sediments. *Geological Society, London, Special Publications 18*, 49–65.
Meyers, W.J. 1977: Chertification in the Mississippian Lake valley formation, Sacramento Mountains, New Mexico. *Sedimentology 24*, 75–105.
Milliken, K.L. 1979: The silicified evaporite syndrome–two aspects of silicification history of former evaporite nodules from southern Kentucky and northern Tennessee. *Journal of Sedimentary Research 49*, 245–256.
Moore, D.M. & Reynolds, R.C. Jr., 1997. *X-Ray Diffraction and the Identification and Analysis of Clay Minerals*, 2nd edn, xviii + 378 pp. Oxford, New York: Oxford University Press.
Morris, S.C. 2009: A redescription of a rare chordate, Metaspriggina walcotti Simonetta and Insom, from the Burgess Shale (Middle Cambrian), British Columbia, Canada. *Journal of Paleontology 82*, 424–430.
Mount, J.F. & Signer, P.W. 1985: Early Cambrian innovation in shallow subtidal environments: paleoenvironments of early Cambrian shelly fossils. *Geology 13*, 730–733.
Muscente, A.D., Hawkins, A.D. & Xiao, S. 2014: Fossil preservation through phosphatization and silicification in the Ediacaran Doushantuo Formation (South China): a comparative synthesis. *Palaeogeography, Palaeoclimatology, Palaeoecology 434*, 46–62.
Noble, J.P.A. & Van Stempvoort, D.R. 1989: Early burial quartz authigenesis in Silurian platform carbonates, New Brunswick, Canada. *Journal of Sedimentary Research 59*, 65–76.
Orr, P.J., Briggs, D.E. & Kearns, S.L. 1998: Cambrian Burgess Shale animals replicated in clay minerals. *Science 281*, 1173–1175.
Page, A., Gabbott, S., Wilby, P. & Zalasiewicz, J. 2008: Ubiquitous Burgess Shale-style 'clay templates' in low-grade metamorphic mudrocks. *Geology 36*, 855–858.
Patwardhan, S.V., Tilburey, G.E. & Perry, C.C. 2011: Interactions of amines with silicon species in undersaturated solutions leads to dissolution and/or precipitation of silica. *Langmuir 27*, 15135–15145.
Peel, J.S. & Ineson, J.R. 2011: The extent of the Sirius Passet Lagerstätte (early Cambrian) of North Greenland. *Bulletin of Geosciences 86*, 535–543.
Perry, C.C. & Keeling-Tucker, T. 2003: Model studies of colloidal silica precipitation using biosilica extracts from *Equisetum telmateia*. *Colloid & Polymer Science 281*, 652–664.
Plint, A.G. 2014: Mud dispersal across a Cretaceous prodelta: storm-generated, wave-enhanced sediment gravity flows inferred from mudstone microtexture and microfacies. *Sedimentology 61*, 609–647.
Powell, W. 2003: Greenschist-facies metamorphism of the Burgess Shale and its implications for models of fossil. *Canadian Journal of Earth Sciences 40*, 13–25.

Raiswell, R. & Berner, R.A. 1986: Pyrite and organic matter in phanerozoic normal marine shales. *Geochimica et Cosmochimica Acta 50*, 1967–1976.
Rajaibi, I.M., Hollis, C. & Macquaker, J.H. 2015: Origin and variability of a terminal proterozoic primary silica precipitate, athel silicilyte, South Oman Salt Basin, Sultanate of Oman. *Sedimentology 62*, 793–825.
Reineck, H.E. & Singh, I.B. 1980: *Tidal Flats. I Depositional Sedimentary Environments*, pp. 430–456. Springer, Berlin, Heidelberg.
Rickard, D.T. 1970: The origin of framboids. *Lithos 3*, 269–293.
Rickert, D., Schlüter, M. & Wallmann, K. 2002: Dissolution kinetics of biogenic silica from the water column to the sediments. *Geochimica et Cosmochimica Acta 66*, 439–455.
Schieber, J. 1996: Early diagenetic silica deposition in algal cysts and spores: a source of sand in black shales? *Journal of Sedimentary Research 66*, 175–183.
Schieber, J., Krinsley, D. & Riciputi, L. 2000: Diagenetic origin of quartz silt in mudstones and implications for silica cycling. *Nature 406*, 981–985.
Schultze-Lam, S., Ferris, F.G., Konhauser, K.O. & Wiese, R.G. 1995: In situ silicification of an Icelandic hot spring microbial mat: implications for microfossil formation. *Canadian Journal of Earth Sciences 32*, 2021–2026.
Seyedolali, A., Krinsley, D. & Boggs, S. 1997: Provenance interpretation of quartz by scanning electron microscope–cathodoluminescence fabric analysis. *Geology 25*, 787–790.
Silva, S.M. & Pienaar, R.N. 2000: *Benthic Marine Cyanophyceae from Kwa-Zula Natal, South Africa*. Gebruder Borntraeger Verlagsbuchland Lung, Berlin, 456 pp.
Stal, L.J. & Walsby, A.E. 2000: Photosynthesis and nitrogen fixation in a cyanobacterial bloom in the Baltic Sea. *European Journal of Phycology 35*, 97–108.
Thickpenny, A. & Leggett, J.K. 1987: Stratigraphic distribution and palaeo-oceanographic significance of European early Palaeozoic organic-rich sediments. *Geological Society, London, Special Publications 26*, 231–247.
Totten, M.W. & Blatt, H. 1993: Alterations in the non-clay-mineral fraction of pelitic rocks across the diagenetic to low-grade metamorphic transition, Ouachita Mountains, Oklahoma and Arkansas. *Journal of Sedimentary Research 63*, 899–908.
Towe, K.M. 1996: Fossil preservation in the Burgess Shale. *Lethaia 29*, 107–108.
Weeks, S.J., Currie, B. & Bakun, A. 2002: Massive emissions of toxic gas in the Atlantic. *Nature 415*, 493–494.
Whittington, H.B. 1980: The significance of the fauna of the Burgess Shale, Middle Cambrian, British Columbia. *Proceedings of the Geologists' Association 91*, 127–148.
Yee, N., Phoenix, V.R., Konhauser, K.O., Benning, L.G. & Ferris, F.G. 2003: The effect of cyanobacteria on silica precipitation at neutral pH: implications for bacterial silicification in geothermal hot springs. *Chemical Geology 199*, 83–90.
Zhu, M., Babcock, L. & Peng, S. 2006: Advances in Cambrian stratigraphy and paleontology: integrating correlation techniques, paleobiology, taphonomy and paleoenvironmental reconstruction. *Paleoworld 15*, 217–222.
Zhu, X., Lerosey-Aubril, R. & Esteve, J. 2014: Gut content fossilization and evidence for detritus feeding habits in an enrolled trilobite from the Cambrian of China. *Lethaia 47*, 66–76.

Supporting Information

Additional Supporting Information may be found in the online version of this article:

Table S1. Results from EDAX (sample 4.56) silt-rich facies converted to oxides using INCA processing software.

Table S2. EDAX spectra from sample 1.12 m from the spotted facies converted to oxides using INCA processing software.

Table S3. EDAX spectra data from the mat material (taken from a cross section through an epirelief cast of *Buenellu*) from sample 340.103a.

Fig. S1. Graphic log of the Buen Formation at Sirius Passet.

Fig. S2. XRD plot of 2θ against intensity with labels showing normalized peaks for each main clay mineral, interpreted using Moore and Reynolds (1997). These data are from sample 0.06 which is the 'lozenge rich' facies.

Fig. S3. XRD plot of 2θ against intensity with labels showing normalized peaks for each main clay mineral, interpreted using Moore and Reynolds (1997). These data are for sample 4.56, the 'mud-rich' facies.